

NAL 60CM MAGNETIC SUSPENSION AND BALANCE SYSTEM

Hideo Sawada, Shinichi Suda, Tetsuya Kunimasu
JAXA, the Institute of Space Technology and Aeronautics (ISTA)

Keywords: *Wind tunnel tests, balance, support, control, drag*

Abstract

A 60cm Magnetic Suspension and Balance System has been developed at JAXA. Magnetic force on a model including rolling moment is controlled with currents through 10 coils around test section of the MSBS. Force calibration test results show error is almost less than 1% FS. Basic controller of the MSBS is PI and a double phase advancer. Newly added controllers suppress interference between motions in x -axis and around y -axis, and also improve model motion much more rapidly by adding magnetic field feedback loop. Support interference of an airship model, drag coefficients of several axis-symmetric shapes and Reynolds number dependency in sphere drag and base pressure using the MSBS are presented.

1. Introduction

A Magnetic Suspension and Balance System (MSBS) provides an ideal way of supporting a model for wind tunnel test because force to support the model is generated by the magnetic field which is controlled by coils arranged outside test section as shown in Fig. 1. Any mechanical support system is not needed in flow field. Then the support interference problem does not exist if using the MSBS.

A 10cm MSBS has been developed since 1985 [1] and a 60cm MSBS has been also developed since 1993 at JAXA/ISTA [2],[3]. It has the largest test section of the world at present. The MSBS was named NAL (National Aerospace Laboratory) 60cm MSBS but the name is changed to JAXA 60cm MSBS according to the new organization name.

The 60cm MSBS was installed in a low-speed wind tunnel. Wind tunnel testing technique with the MSBS has been examined [4]. Magnetic field, control system and some aerodynamic test results at the MSBS are described in this paper.

2. JAXA 60cm MSBS

2.1 Magnetic Force Control and Coil Arrangement

Magnetic force, F and N , acting on a model for wind tunnel test at the MSBS can be evaluated by the following expressions,

$$\begin{aligned} F &= (M \cdot \nabla)H, \\ N &= M \times H, \end{aligned} \quad (1)$$

when the model has magnetic moment of M . H means magnetic field intensity around the model. The model for the JAXA 60cmMSBS

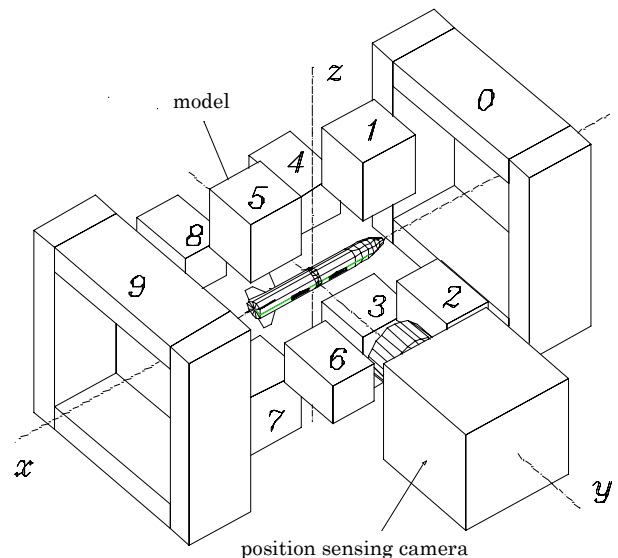


Fig. 1. JAXA MSBS Coil Arrangement

has a permanent cylindrical magnet in it which is parallel to model axis.

In order to control the field, various electric magnet arrangements have been proposed [5]. Figure 1 is the arrangement of JAXA MSBS. The 60cm MSBS consists of 8 electromagnets and 2 air cored coils. The coordinate system is also depicted in Fig.1. The model is located at the origin of the system. If the model is on the x -axis, \mathbf{M} has only x component. Then, Eq. (1) becomes

$$F_x = M_x \frac{\partial H_x}{\partial x}, \quad F_y = M_x \frac{\partial H_y}{\partial x}, \quad F_z = M_x \frac{\partial H_z}{\partial x}, \quad (2)$$

$$N_x = 0, \quad N_y = -M_x H_z, \quad N_z = -M_x H_y.$$

Pitching moment, N_y and lift force, F_z can be controlled by adjusting H_z and its x derivative according to Eq. (2). Then, the upper and lower coils in Fig.1, #1, #3, #5, and #7, are combined into two sets, (#1+#3) and (#5+#7), and currents through the combined coils are controlled to generate H_z and its x derivative with two power units which can provide the coils with 120A continuously in maximum. When the same current (lift current, I_{lift}) passes through the combined coils, x derivative of H_z generates as shown in Fig.2. The figure shows specific z -components of \mathbf{H} per unit I_{lift} , h_z 's, vs. x in six lift current cases. The six h_z 's are in agreement with each other. The x derivative of h_z is independent of I_{lift} approximately and has constant gradient around model center. Then the x derivative can be expressed approximately with 3rd expression of Eq. (3). I_i in Eq. (3) is coil current through coil, # i . F_z is proportional to I_{lift} .

When current (pitch current, I_{pitch}) through coil, (#1+#3) has the same magnitude but opposite sign as the current through coil,

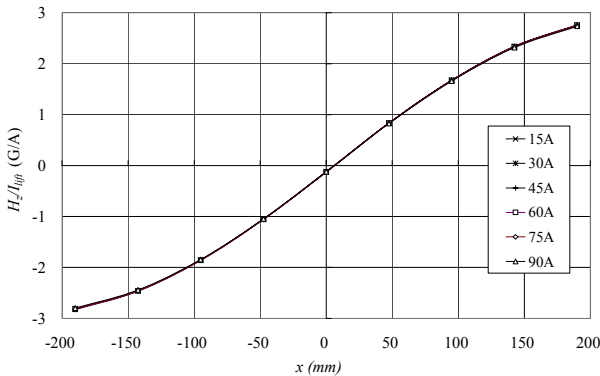


Fig.2 h_z vs. x in Lift Current Change

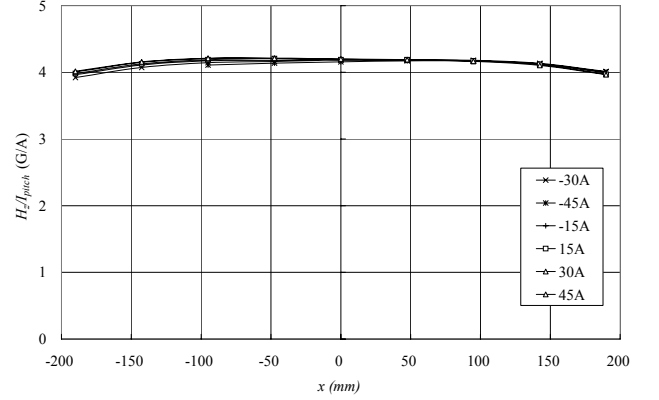


Fig.3 h_z vs. x in Pitch Current Change

(#5+#7), I_{pitch} generates H_z which does not vary in x direction as shown in Fig.3. As in the case of lift current, H_z can be expressed approximately with 5th expression of Eq. (3). N_y is proportional to I_{pitch} .

Similarly, F_x , F_y and N_z are proportional to I_{drag} , I_{side} and I_{yaw} , respectively, as are expressed in Eq. (3).

$$\frac{\partial H_x}{\partial x} = h_{xx} \cdot I_{drag},$$

$$\frac{\partial H_y}{\partial x} = h_{yx} \cdot I_{side},$$

$$\frac{\partial H_z}{\partial x} = h_{zx} \cdot I_{lift},$$

$$H_y = h_y \cdot I_{yaw},$$

$$H_z = h_z \cdot I_{pitch}, \quad (3)$$

$$I_{dragt} = (I_0 + I_9) / 2,$$

$$I_{side} = (I_2 + I_4 + I_6 + I_8) / 4,$$

$$I_{lift} = (I_1 + I_3 + I_5 + I_7) / 4,$$

$$I_{yaw} = (I_2 + I_4 - I_6 - I_8) / 4,$$

$$I_{pitch} = (I_1 + I_3 - I_5 - I_7) / 4.$$

Each of four side coils is driven with a power unit, respectively. The side coils of #2,

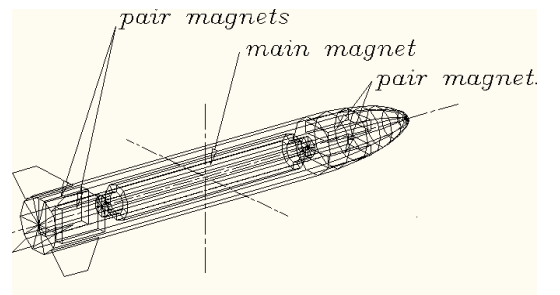
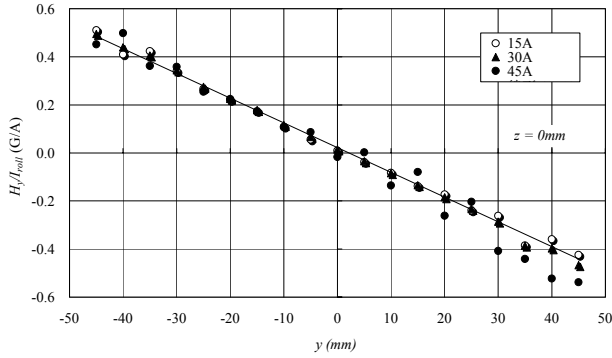


Fig. 4 A Roll Control Model


 Fig.5 h_y vs. y in I_{roll} Change

#4, #6, and #8 control H_y and its x derivative. Currents of the four power units range from -60A to 60A in steady condition. The MSBS can act rolling moment on a special model with pair magnets as shown in Fig.4 by controlling the four side coil currents independently. H_y of acting rolling moment on the model is shown in Fig.5. The measured specific rolling moment is depicted in Fig.6 with designed figures. The moment depends on the roll angle ϕ . The roll current follows:

$$I_{roll} = (I_2 - I_4 - I_6 + I_8) / 4. \quad (4)$$

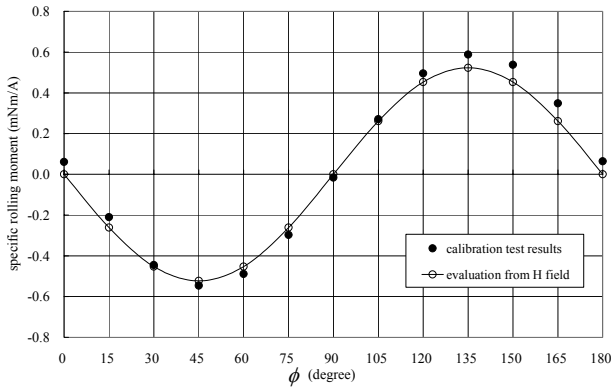


Fig.6 Calibration Test Result of Rolling Moment

coil #	turn number	size	purposes
0,9	50	620 x 620	drag
1,3,5,7	97 + 97	200 x 200	lift, pitching moment
2,4,6,8	100	200 x 200	side force , yawing moment, rolling moment
coil drive units	130V, 120A in continuous mode ... 3 units 130V, 60A in continuous mode ... 4 units		
control	5 DOF for models with a main magnet only 6 DOF for special models with pair magnets		

Table 1 Specifications of the 60cm MSBS

The specifications of the coils and coil drive power units are listed in Table1.

2.2 Aerodynamic Force Measurement

The equation of motion for a magnetically suspended model in flow can be expressed as follows:

$$\frac{d(m\mathbf{v})}{dt} = \mathbf{F}_{magnet} + \mathbf{F}_{aero} + \mathbf{F}_{gravity}, \quad (5)$$

$$\frac{d(\mathbf{I} \cdot \boldsymbol{\omega})}{dt} = \mathbf{N}_{magnet} + \mathbf{N}_{aero} + \mathbf{N}_{gravity},$$

where m and \mathbf{I} are mass and inertia tensor of the model. \mathbf{v} and $\boldsymbol{\omega}$ are translational and angular velocities of its mass center. Subscripts, 'magnet', 'gravity' and 'aero', mean magnetic, gravity and aerodynamic forces, respectively. \mathbf{v} and $\boldsymbol{\omega}$ can be evaluated from model position. The position is measured always at the MSBS and magnetic force is also evaluated from coil currents. Then unknown aerodynamic force can be evaluated with Eq. (5). This is the principle of balance function of MSBS. In case of evaluating acceleration with its measured position, large error will be included due to the 2nd numerical derivative evaluation. Then unsteady aerodynamic force measurement has not been accurate enough yet at the 60cmMSBS. On the contrarily, steady aerodynamic force can be evaluated very accurately by averaging coil currents for long time. If both sides of the above expression are averaged for long time of T , following equations are obtained:

$$m \frac{\mathbf{v}(T) - \mathbf{v}(0)}{T} = \frac{1}{T} \int_0^T (\mathbf{F}_{magnet} + \mathbf{F}_{aero}) dt + \mathbf{F}_{gravity}, \quad (6)$$

$$\frac{1}{T} [\mathbf{I} \cdot \boldsymbol{\omega}]_0^T = \frac{1}{T} \int_0^T (\mathbf{N}_{magnet} + \mathbf{N}_{aero}) dt + \mathbf{N}_{gravity}$$

The magnitude of model velocity and angular momentum can be suppressed within a certain value quite easily if model position control goes well. Then, averaging coil currents for long time makes the left hand sides of Eq. (6) negligible. When the model is suspended magnetically in no flow at the same position as in flow, subtracting magnetic force in no flow from that in flow gives only aerodynamic force without any gravity force information. Accuracy

of aerodynamic force depends on evaluation of the magnetic force only.

		Kind of Control Current				
		I_{drag}	I_{side}	I_{lift}	I_{pitch}	I_{yaw}
force	range	220.0A	98.5A	80.8A	80.1A	98.5A
F_x	24.6N	0.4%	0.4%	0.2%	0.7%	1.2%
F_y	40.1N	0.1%	1.0%	0.1%	0.4%	0.8%
F_z	61.6N	0.4%	0.4%	1.1%	1.2%	1.2%
N_y	14.7Nm	0.3%	0.3%	0.5%	0.8%	0.2%
N_z	9.1Nm	0.0%	0.0%	0.0%	0.0%	0.9%

Table2 JAXA 60cmMSBS Error Evaluation

2.3 Balance Calibration Results

It is difficult to measure the magnetic moment of a model for wind tunnel test accurately. Then the magnetic force evaluation from Eq. (1) would include large error. It is much more accurate to evaluate the force with a directly calibrated relation between magnetic force and

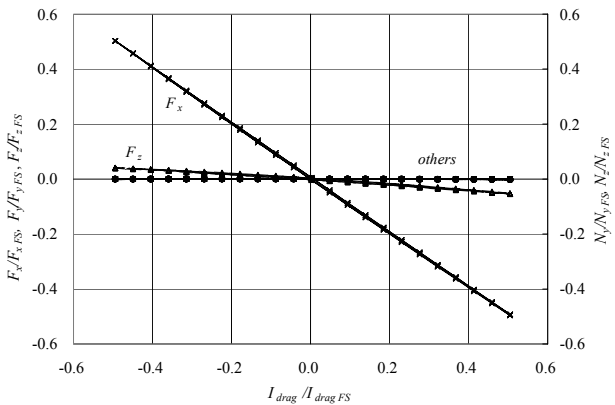


Fig.7 Calibration Test Result in Drag Load

Alnico 5 permanent one which is 55 mm in diameter and 235 mm long. Balance calibration test results indicate the error in each component is about 1% in full range as shown in Table 2. An example of drag calibration test result is shown in Fig.7. It shows good linearity but a little hysteresis phenomenon. If support interference correction is expected to be larger than that in Table 2, use of the MSBS would be recommended to carry out reliable wind tunnel tests.

2.4 Control System of the 60cm MSBS

2.4.1. Fundamental Control System

The present control system employed in the 60cm MSBS is shown in Fig. 8. In this figure, a decoupling controller and a magnetic field feedback controller mentioned later are include, and fundamental elements are parts excluding elements enveloped in dashed lines. At first, the position and attitude of the model are measured by two optical sensors. Sampling frequency and control frequency are both 248 Hz. Dead time of the optical sensors is about 6 msec.

$$H_s(s) = e^{-Ls}, \quad L = 0.006 \quad (7)$$

Sensor noise is eliminated by a second-order Butterworth filter of cut-off frequency of 10 Hz.

$$H_n(s) = \frac{\omega_c^2}{s^2 + \sqrt{2}\omega_c s + \omega_c^2} \quad (8)$$

where $\omega_c = 2\pi \times 10$ rad/sec. However, the measured position and attitude of the model has

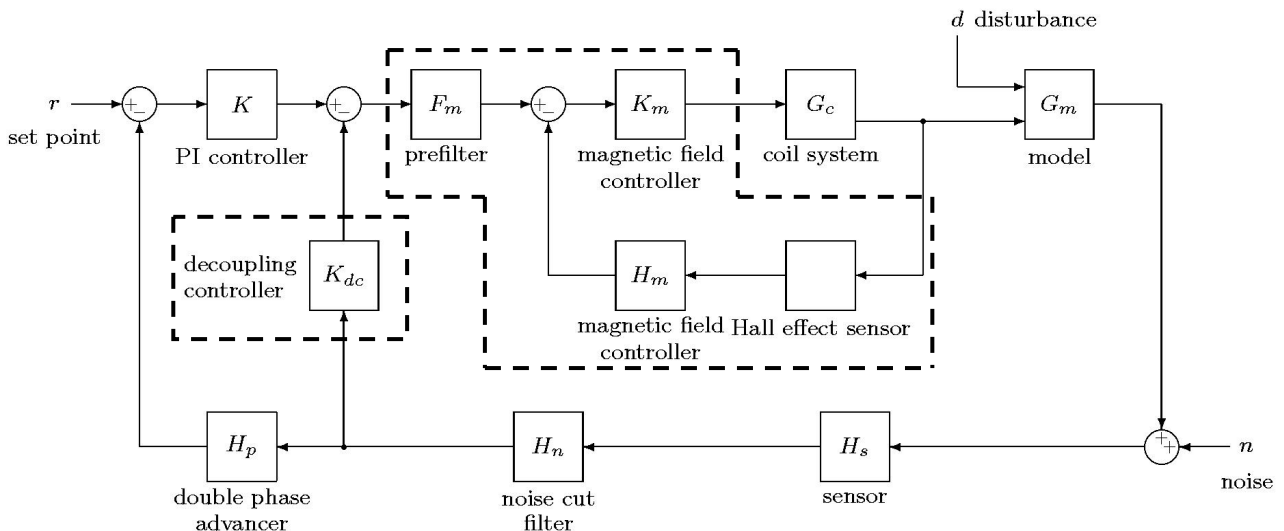


Fig.8. 60cm MSBS Control System

$$H_p(s) = \left(\frac{p_b s + 1}{p_a s + 1} \right)^2, \quad (9)$$

$$p_b = \frac{2n_p T_p + T_s \times 10^3}{2 \times 10^3},$$

$$p_a = \frac{2T_p + T_s \times 10^3}{2 \times 10^3}$$

where T_s is a sampling time. Furthermore, a proportional-integral (PI) controller is employed to vanish errors between the compensated position and attitude and the objective set-points.

$$K(s) = k_p \left(1 + \frac{1}{T_i s} \right) \quad (10)$$

Calculated control currents are converted into magnetic force through the coil system.

2.4.2. Elimination of Coupling Motion

In the 60cm MSBS, motions of y , z , ψ axes are regarded as independent. On the other hands, there is a coupling motion problem between x

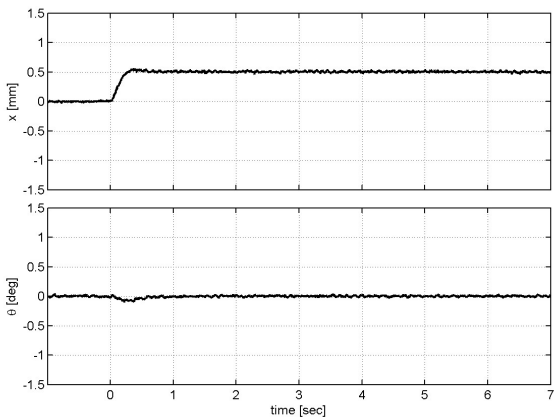
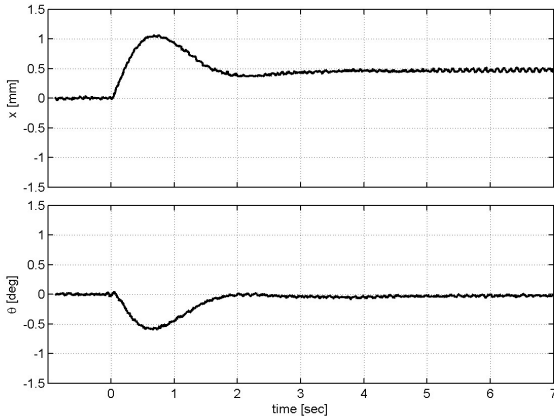


Fig.9. Experimental Results of Decoupling Control

and θ axes, that is, when one axis is excited, the other axis is also excited. Coupling motions of a cylinder model (mass: 1.345 kg, length: 186 mm, diameter: 45 mm) are shown in the upper part of Fig.9. When x steps, θ deviates from the set point. Similarly, when θ steps, x also deviates. These coupling motions cause unexpected motion of the model and destabilize the stability of the model in motion. Furthermore, there is wrong effect on evaluation of forces and moments. Thus, elimination of the coupling motions is necessary.

To eliminate such coupling motion, control current depending the position and attitude of the model is added to the fundamental control current [7], that is,

$$\begin{cases} I_{drag}(t) = I_{drag}^0(t) + \frac{mg}{M_x h_{zx}} \theta(t) \\ I_{pitch}(t) = I_{pitch}^0(t) - \frac{mg}{M_x h_z} x(t) \end{cases} \quad (11)$$

where I_{drag}^0 , I_{pitch}^0 are the control current calculated by the fundamental control system, g is the gravity constant. The control system block diagram is a part combining the fundamental control system and the decoupling controller K_{dc} in Fig. 8.

In the case of the cylinder model mentioned above, coefficients multiplied θ and x in Eq. (11) are 7.61 A/deg and 0.26 A/mm, respectively. On the other hands, these coefficients are obtained experimentally as shown in Fig. 10. This figure is obtained by measuring the steady control current when varying θ and x , and gradients in Fig. 10, $I_x/\theta = 8.46$ A/deg and $I_\theta/x = 0.31$ A/mm, correspond the coefficients in Eq. (11). Since there are some parameter errors in Eq. (11), gradients obtained experimentally is appropriate for the actual system, and more effective than the theoretical values.

An experimental result of the decoupling controller is shown in the lower part of Fig. 9. It is shown that coupling motion between x and θ is drastically eliminated. Furthermore, the overshoot of x vanishes. In this experiment, the control parameters of the PI controller and the double phase advancer are set in the identical

values that are used in the fundamental control system. The control parameters in the fundamental control system are designed under the assumption that the system is a single-input single-output (SISO) system. Thus, the results of the decoupling control imply that the decoupled system is successfully regard as SISO system. Because of the decoupling controller, the stability of the system is improved, and dynamic tests can be examined in stable condition, where several axes are activated simultaneously, for instance oscillating heaving and pitching simultaneously.

2.4.3. Rapid Magnetic Field Feedback Control Using Hall Effect Sensors

In the 60cm MSBS, it has been pointed out that there is a little delay between the control current and the response of the model. The reason is that formation of the magnetic field needs a little time because of the coil inductance. This delay is small and there is no bad influence in the static tests. However, this delay becomes a

problem in future when increasing the control frequency, or when testing in high subsonic flow. On the other hands, it has been confirmed by measurement using the Hall effect sensors that the response of the model and the response of the magnetic field are in phase. Accordingly, it is expected that more rapid control of the model is accomplished by adding a magnetic field feedback control.

Eleven Hall effect sensors are equipped in the 60cm MSBS, and it is necessary to relate the outputs of the Hall effect sensors to values indicating the magnetic field along each control axis. In case of relating the Hall effect sensor outputs in the same way as control currents, Eq. (3), it is confirmed that the evaluated values can be used for the magnetic field feedback control. For example, a measurement result of H_{drag} , H_{side} , H_{lift} , H_{pitch} , H_{yaw} when varying the control current I_{side} is shown in Fig.11. In this figure, only H_{side} varies larger than the other values and the others do not almost vary. H_{side} can be adopted as the value indicating the magnetic field of y direction.

The magnetic field feedback control is introduced into the 60cm MSBS control system as an inner loop, as shown in Fig. 8 [8]. The magnetic field formed by the coil system G_c is measured by the Hall effect sensors, and H_{drag} , ..., H_{yaw} are calculated in H_m , and fed back. K_m is the magnetic field feedback controller, and F_m is a prefilter to unify the dimensions of the values. In the 60cm MSBS, the coil systems G_c in each axis have been identified as the products of a first-delay element and a few phase delay elements. For example, the transfer function of

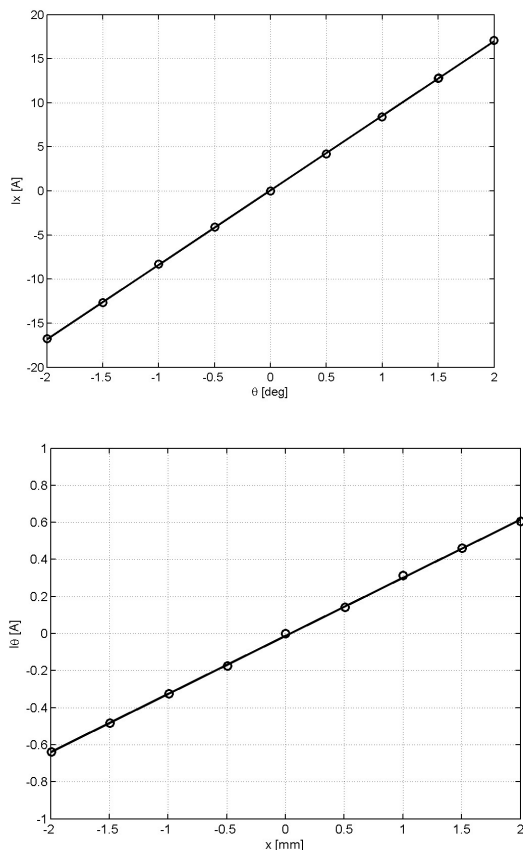


Fig.10. Calibration of Coupling Effect

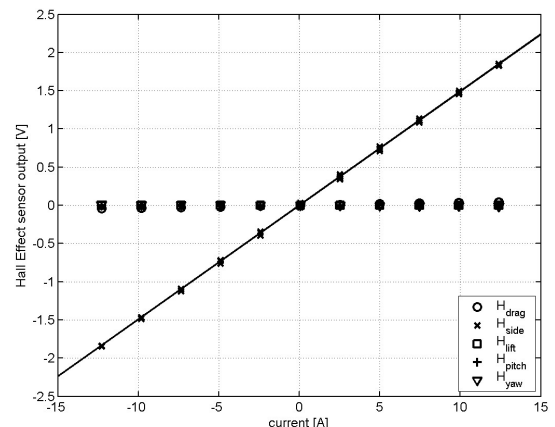


Fig.11. Hall Effect Sensor Output

the coil system in y direction is represented as

$$G_c(s) = \frac{1}{s/715+1} \frac{s/93.5+1}{s/73.7+1} \frac{s/3.71+1}{s/3.09+1}, \quad (12)$$

where the gain of G_c is normalized so that $G_c(j\omega) \rightarrow 1$ when $\omega \rightarrow 0$.

To explain the way to design the magnetic field feedback controller, now consider the simplest coil system model as follows:

$$G_c(s) = \frac{1}{s/a_0+1} \frac{s/b_1+1}{s/a_1+1} \quad (13)$$

where $a_0 > b_1 > a_1$. Although the coil system includes phase delays expressed as Eq. (13), if the time constant $1/a_0$ and the difference of b_1 and a_1 are small enough, there is no matter in practice. Thus, the aim of the controller design is to find a controller to reduce the time constant and the phase delay of the closed-loop coil system. One of the controllers that can achieve the aim is a constant controller, that is, $K_m = \text{const}$, $H_m = \text{const}$, and $F_m = \text{const}$. For example, the closed-loop transfer function of the coil system in y direction was designed as

$$M_{cl}(s) = \frac{1.65}{s/1170+1} \frac{s/93.5+1}{s/82.1+1} \frac{s/3.71+1}{s/3.38+1}, \quad (14)$$

and it is shown that the time constant and the phase delay are decreased comparing Eqs. (12) and (14).

An experimental result of the magnetic field feedback controller is shown in Fig.12, where a solid line is the step response in the case including the magnetic field feedback control, and a broken line the step response in

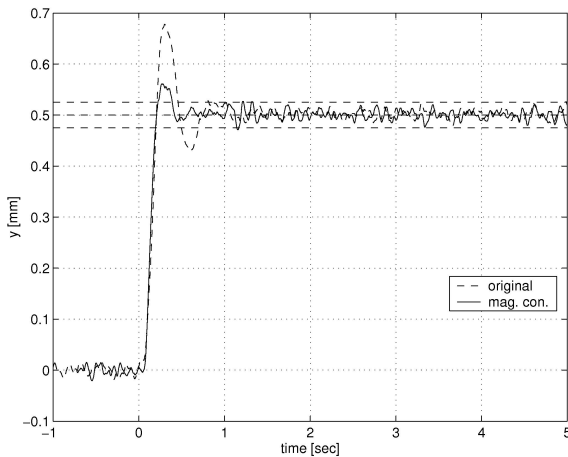


Fig.12. Experimental Result of Magnetic Field Feedback Control

the case of the fundamental control system. The settling time of the fundamental control system is 0.70 sec, and that of the magnetic field feedback control is 0.40 sec. Due to the magnetic field feedback control, the settling time can be reduced drastically. It is expected that the magnetic field feedback control is very useful when the control frequency is increased, or when tests in high subsonic flow.

3. JAXA 60cm MSBS Wind Tunnel

The MSBS was installed at the 60cm x 60cm low speed wind tunnel in 1999. The tunnel circuit is depicted in Fig. 13. The MSBS test section replaced the downstream part of the test section. A new collector was designed and installed to meet the new situation of the tunnel. The low speed wind tunnel test section with the 60cm MSBS is shown in Fig.14.

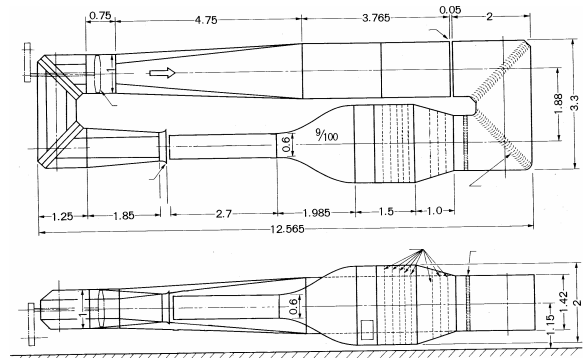


Fig.13. Low Speed Wind Tunnel for the JAXA 60cm MSBS (unit: m)



Fig.14. Test Section and the JAXA 60cm MSBS

The flow quality has been examined two times. The MSBS test section has the constant cross section along the flow, and then the flow is accelerated due to the boundary layer development. The flow speed was calibrated at the center of the MSBS test section. The available flow speed ranges from 10 to 35 m/s. The measured flow angle at the center is 0.05 degree in downwash and 0.15 degree about z-axis shown in Fig. 1. The pressure coefficient gradient is $-0.03/m$. The fluctuation ratio of flow speed is less than 0.05% in rms value in the range to 20kHz. Flow quality and the tunnel specifications are listed in Table 3.

test section	0.6m wide, 0.6m high, 1.2m long
fan drive unit	11 kW
contraction ratio	11.1
flow speed	10 ~ 35 m/s
pressure gradient	$-0.03 /m$ in pressure coefficient
flow angles	0.05 deg. downwash 0.15 deg. rotate about z-axis
turbulence intensity	less than 0.05%

Table 3. The JAXA 60cm MSBS Wind Tunnel

4. Support Interference Evaluation

One of the purposes of equipping the tunnel with the MSBS was to estimate the support interference in a new airship development project at JAXA. The drag of airship consists of friction and pressure drags. The boundary layer transition and flow separation affect on the two kinds of drag, sensitively. The flow is very complicated around the connecting section between the support and model. It is afraid whether or not the well-known simple subtraction method of evaluating the interference could be still available in this sensitive case. It is easy to estimate the model drag in the interference free if the drag is measured with the MSBS. A 4 to 1 ellipsoid model was used to estimate the support interference. Its diameter is 90mm and it is 360mm long and its mass is around 5.4kg.

The support interference on the drag coefficient can be evaluated easily by comparing between the measured coefficients in

no strut case and in a dummy strut case. Figure 15 shows the model at test section in both test cases. Figure 16 shows the obtained test result. The gap between model and dummy strut was fixed at 0.25mm in this case. It suggests the interference depends on Reynolds number in tested case. Details must be referred to [9].

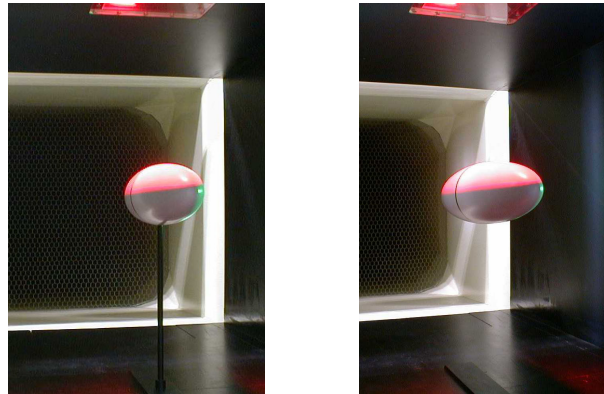


Fig. 15. Support Interference Test Model Magnetically Suspended in Test Section

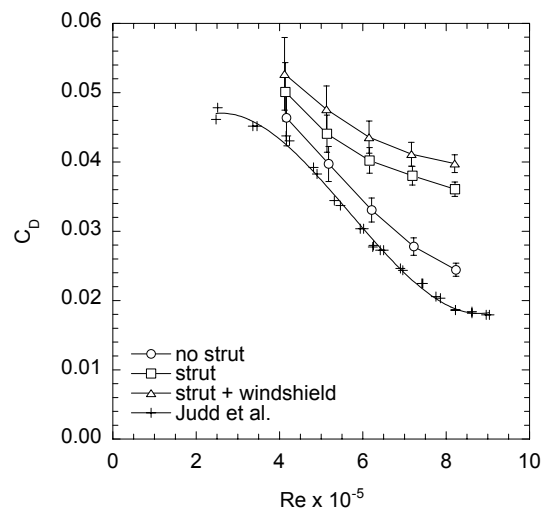


Fig. 16. Support Interference Test with a 4 to 1 Ellipsoid Model

5. Drag Measurements of Fundamental Shapes with the 60cm MSBS

Drag coefficients of several axis-symmetric shapes have been evaluated with the MSBS which are listed in Table 4. The values are all support interference free. Some of them are compared with other reliable data sets in order to estimate the reliability of our drag measurement technique with the MSBS. Some are good

agreement with other source data sets which are measured with any mechanical support. But some are different from other source. We are planning to add the coefficients of other fundamental shapes. A 6:1 cone model suspended magnetically is shown in Fig. 17.

name	Drag coefficient	Other source	Reynolds number	Representative length
6:1 ellipsoid	0.05 to 0.06	[10]	100000	length
6:1 cone	0.20 to 0.24	none	100000	length
5:1 axial cylinder	0.88 to 0.90	[11]	100000	diameter
sphere	0.43	[12]	350000	diameter
4:1 axial cylinder	0.865	[11],[12]	100000	diameter
Cone cylinder	0.217	none	80000	length

Table 4. Shapes Tested at the JAXAL 60cm MSBS Wind Tunnel

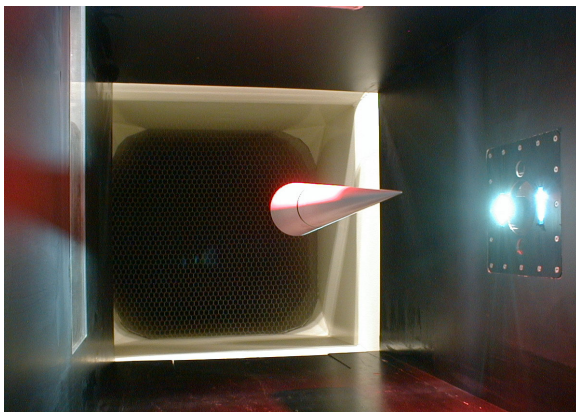


Fig. 17. A 6 to 1 Cone Model Suspended in the 60cm MSBS

6. Drag and base pressure coefficients of sphere

Drag coefficient of sphere has been one of the most interesting subjects for aerodynamic researchers. Many obtained data sets were reported as shown in Fig.18 [12], [13]. But it is very difficult to measure it accurately due to support interference. Using the MSBS provides with drag coefficient in the interference free [14]. The model is 150mm in diameter. Figure 19 shows the model suspended magnetically in the MSBS. The obtained data set with the MSBS shows the critical Reynolds number is

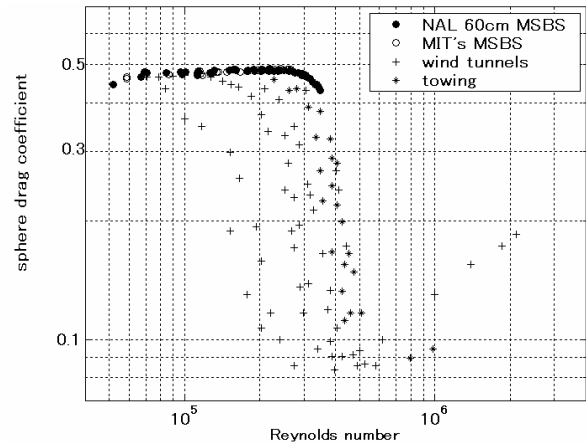


Fig.18 Reynolds Number vs. Sphere Drag Coefficient larger than other data sets with mechanical supporting systems.

Base pressure is very sensitive on sphere drag because it has large wake. The effect of the sting to support a sphere model has not been evaluated yet. We measured the pressure with telemeter system inside the model without the interference free completely as shown in Fig.20. The base pressure was measured with reference of stagnation pressure. The obtained base

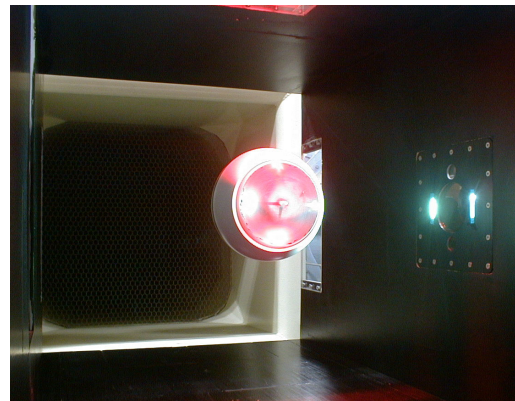


Fig. 19. The Magnetic Suspended Sphere Model



Fig.20 Telemeter System in a Sphere Model

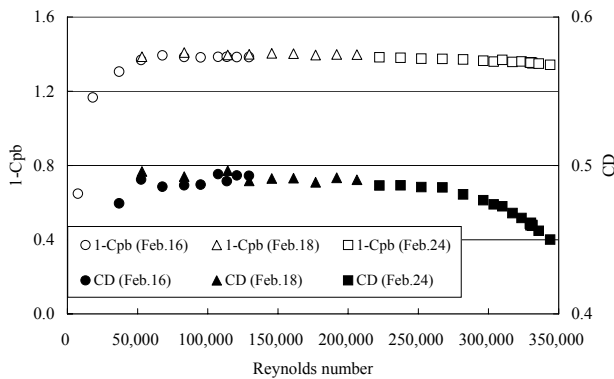


Fig.21 C_D and Base Pressure Coefficient vs. Reynolds Number

pressure coefficients were depicted vs. Reynolds number in Fig.21. The ratio of obtained pressure coefficient to drag coefficient keeps constant approximately up to around Reynolds number of 250000. But the ratio increases as Reynolds number increases beyond the value [15].

7. Remarks

60cm Magnetic Suspension and Balance System has been developed in JAXA. Magnetic field and control system are described. Besides, some aerodynamic test results using the MSBS are presented. Especially,

- Magnetic force on a model including rolling moment is controlled with coil currents through 10 coils arranged around test section of the MSBS. Force calibration test results show error is less than 1% FS.
- Fundamental control of the MSBS is PI and a double phase advancer. Newly introduced control systems suppress interference between motions in x -axis and around y -axis and improve model motion much more rapidly with adding magnetic field feedback loop.
- Evaluated support interference with the MSBS is reliable because it is directly measured.
- Drag coefficients of several axis-symmetric shapes and Reynolds number dependency of sphere drag and base pressure using the MSBS are very valuable because they are measured in sting interference free.

References

- [1] Sawada H, Kanda H and Suenaga H. The 10cm x 10cm magnetic suspension and balance system at the National Aerospace Laboratory. *AIAA 91-0397*, 1991.
- [2] Sawada H and Suenaga H. Status of MSBS study at NAL. *NASA CP 3247*, pp 275-289, 1994
- [3] Sawada H, Suenaga H and Kohno T. Status of MSBS study at NAL in 1995. *NASA CP 336*, pp 505-519, 1996.
- [4] Sawada H and Kunimasu T. Development of a 60cm magnetic suspension system. *J. Japan Society for Aeronautics and Space Science*, Vol. 50, No. 580, pp 188-195, 2002.
- [5] Covert E E, Finston M, Vilajinac M and Stephens T. Magnetic balance and suspension systems for use with wind tunnels. *Progress in Aerospace Science*, Vol.14, pp 27-107, 1973.
- [6] Sawada H, Kunimsu T, Suda S, Mizoguti Y, Okada T. 5-Axis force calibration test results for the JAXA 60cm MSBS. *J. Japan Society for Aeronautics and Space Science*, Vol. 52, No. 606, pp 309-315, July, 2004.
- [7] Suda S, Sawada H and Kunimasu T. Decoupling control to reduce the coupling effect for NAL magnetic suspension and balance system. *Proceedings of the 15th Symposium on Electromagnetics and Dynamics*, pp 467-470, 2003
- [8] Suda S, Sawada H and Kunimasu T. Improvement of control performance for NAL magnetic suspension and balance system by adding a magnetic field feedback loop. *Proceedings of the 45th Japan Automatic Control Conference*, pp 373-376, 2002
- [9] Harada K, Sawada H and Takahashi H. Support-interference effects on airship wind tunnel testing. *Proceedings of the 32nd JSASS Annual Meeting*, March, 2001.
- [10] Judd M, Vlajinac M and Covert E E. Sting-free drag measurements on ellipsoidal cylinders at transition Reynolds numbers. *J. Fluid Mechanics*, Vol.48, Part 2, pp 353-364, 1971.
- [11] Roberson J A and Crowe C T. *Engineering fluid mechanics*. 6th edition, John Wiley & Sons, Inc., 1997.
- [12] Vlajinac M and Covert E E. Sting-free measurements of sphere drag in laminar flow. *J. Fluid Mech.*, vol.54, part3, pp 385-392, 1972.
- [13] Hoerner S F. *Fluid-dynamic drag*. published by author, pp 3-7 – 3-8, 1958.
- [14] Sawada H, Kunimasu T and Suda S. Sphere drag measurement with the NAL 60cm MSBS. *J. of Wind Engineering*, No.98, January, pp 129-135, 2004.
- [15] Sawada H, Kunimasu T, Suda S and Misunou T. Sting-free measurements of sphere base pressure. *Wind Engineers*, No.99, April., pp 145-146, 2004.